

Test Report: Proton Radiation Evaluation of TIRS QWIP and Indigo 9808 Multiplexer

Cheryl Marshall, Roger Foltz, Emily Kan, Greg Delo, Nicholas Boehm, Augustyn Waczynski
April 1, 2009 DCL GSFC

References:

- [1] "Report on the Total Ionizing Dose Radiation Testing of the Indigo 9803 Readout Integrated Circuit for the Thermal Infrared Sensor Instrument," Augustyn Waczynski, Cheryl Marshall, D. Brent Mott, October 30, 2008.

Summary:

Two QWIP arrays hybridized to ICS9803 multiplexers were irradiated by 9 and 63 MeV protons as a part of the space qualification program for the LDCM TIRS instrument focal plane array (FPA). The devices were exposed to a total fluence of 1.5×10^{11} 63.3 MeV protons per cm^2 . The device parameters measured that respond to the total ionizing dose (TID) and displacement damage produced by the proton exposure remained essentially unaffected by the radiation. However, transient effects indicating a sensitivity to single event effects (SEE) were observed during radiation exposures to low proton fluxes. At least two types of SEE effects were captured during high flux proton exposures, one of which required a power cycle to return to normal operation. The proton irradiations and measurements were performed at Crocker Nuclear Laboratory (CNL) accelerator of the University of California in Davis (UC Davis) on Nov. 19 – Nov. 20, 2008.

Further analysis of the SEE response of the QWIP and Indigo 9803 is recommended, in particular as full characterization of the SEE events requiring a power reset to return to normal operation is not complete. In contrast to the evaluation of the proton induced dark current, noise, and responsivity behavior, the SEE analysis requires manual inspection of an exceedingly large number of frames, which will take further efforts to conclude.

Experimental Description:

The primary goal of the experiment was to determine the effects of the proton space environment (due to trapped protons and solar flare protons) on the performance and functionality of the ICS9803 multiplexer and QWIP detector assembly, referred to as the sensor chip assembly (SCA) for the rest of the document. A secondary goal was to explore the response to proton induced nuclear reaction products which have a higher linear energy transfer (LET), and also to evaluate proton transient signatures. The proton energy of 63.3 MeV was selected as the primary test energy since it is representative of a well shielded space application. However, in order to detect transients using the SEIR data acquisition system, we also exposed the SCA to 9 MeV protons which have a significantly higher LET, so that the transient response was more easily detected.

The 5 year mission TID has been estimated as 9 krad(Si), including the NASA mandated factor of two margin for uncertainties in the mission dose calculation. This TID level assumes a nominal shielding thickness of 200 mils Al equivalent. However, the devices were irradiated to a 20 krad(Si) 63 MeV equivalent fluence of 1.5×10^{11} protons per cm^2 in multiple radiation steps. This was done in order to obtain a crude indication of whether the SCA would be sensitive SEE effects produced by higher LET particles, which will be encountered in space in the form of cosmic rays. (See Appendix II for more discussion.) Of course, the effects of high energy proton induced nuclear reactions themselves are also characterized with better statistics as a result of the higher irradiation level. The higher exposure levels were possible because the Indigo 9803 had previously been tested at the GSFC cobalt 60 facility [1], and had demonstrated tolerance to this level of exposure. Also, it was expected that based on the literature, and because the QWIP technology has no oxides, and the dark current requirements for TIRS are not stringent, that the QWIP would also perform well. Before and after each exposure, the device performance was evaluated by measurement of the dark and photo responses. An internal ‘grey body’ source was placed behind the cold shields to provide illumination for the detector. In addition, after each radiation step bias voltages and currents were measured. Images were collected during all irradiation exposures to monitor the detector response to SEE. The results presented here were collected over 3 days of radiation testing at a detector temperature of 40 K while at the UC Davis CNL.

Two engineering QWIP devices (Q115 and Q116) were used for proton testing. These arrays were optimized for an 8.6 μm spectral response. In particular, both Q115 and Q116 were evaluated real time to a series of very low proton flux exposures to characterize their transient response. The low fluxes corresponded to approximately one proton per 100 pixels per 10 ms exposure time at two proton energies: 63.3 MeV and 9 MeV. Successful images were collected at both proton energies, and for several integration times in order to understand the contributions from both the detector and MUX. In addition, both SCAs were exposed to incremental TID steps up to a total exposure level of 20 krad(Si) in order to assess global permanent radiation effects. Images were also collected during the higher flux incremental exposures. See Appendix I, for further dosimetry details.

Test Setup:

Devices were placed inside the cryostat and were operated during all proton exposures at a temperature of 40 K. The cryostat window was removed and replaced with a 0.125 mm thick kapton tape, in order to facilitate penetration of the incident protons. The window in the thermal shield was masked by a 0.025 mm thick aluminum tape. The cryostat was positioned against the end of the proton beam line, and the detector was irradiated by a collimated proton beam that penetrated the dewar through the vacuum and radiation shields. In the case of the low energy proton exposure, the distance from the end of the beam line to the kapton window of the dewar was measured in order to account for the proton energy loss in air.

Two data acquisition systems were used. The SEIR system was employed earlier for cobalt 60 gamma testing [1], and also for the pre-irradiation characterization of the detectors. Since numerous performance problems were identified during those tests, a new data acquisition

system based on a Leach controller was adopted for the SCA just in time for the second day of radiation testing. As a result, most of the work with Q116 was done with the SEIR, whereas during the second day, the Q115 was exclusively tested with the Leach controller. Selected tests were repeated with the Leach controller for Q116 as well. A schematic of the test set-up is illustrated in Fig. 1.

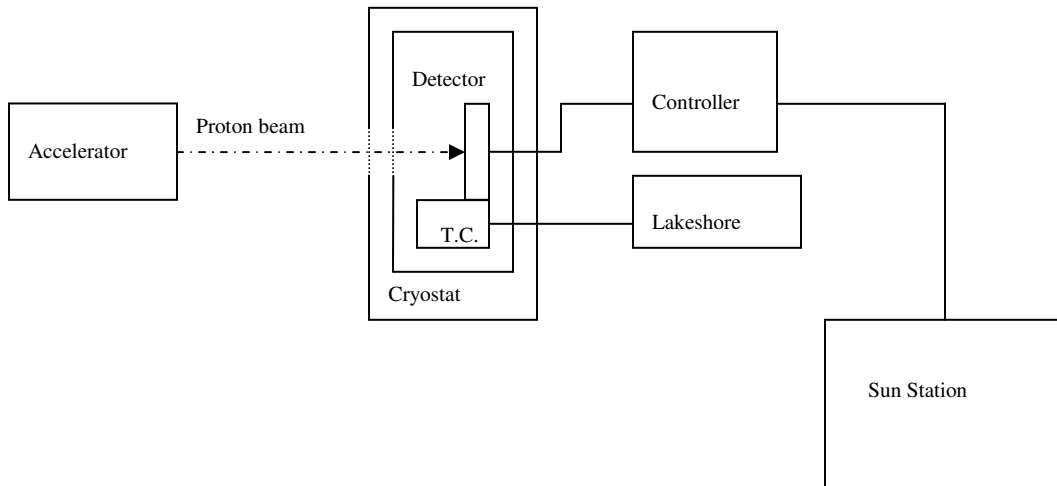


Fig. 1 Radiation test setup. The detector was placed in the cryostat and stabilized at 40 K using a Lakeshore temperature controller. The data acquisition controller was linked to the host computer with a fiber optic link.

Test Results - Dark current:

The dark current and noise remained virtually unchanged over the entire course of the radiation experiment. As shown in Figs. 2 & 3, the dark currents measured before and after irradiation were the same within the error of the measurements. Both detectors exhibited the same behavior. Since the ICS9803 multiplexer is a ‘snap on’ type of multiplexer and does not support a nondestructive readout, multiple images with varying exposure times were collected. The dark current was calculated as a slope of the signal versus exposure time.

The images collected with the SEIR system have random pixel values that are most likely caused by spurious effects in the analog to digital (A/D) converters. These images also show system differential nonlinearities (see Fig. 2). When similar data on the same array was collected with Leach controller these effects were absent.

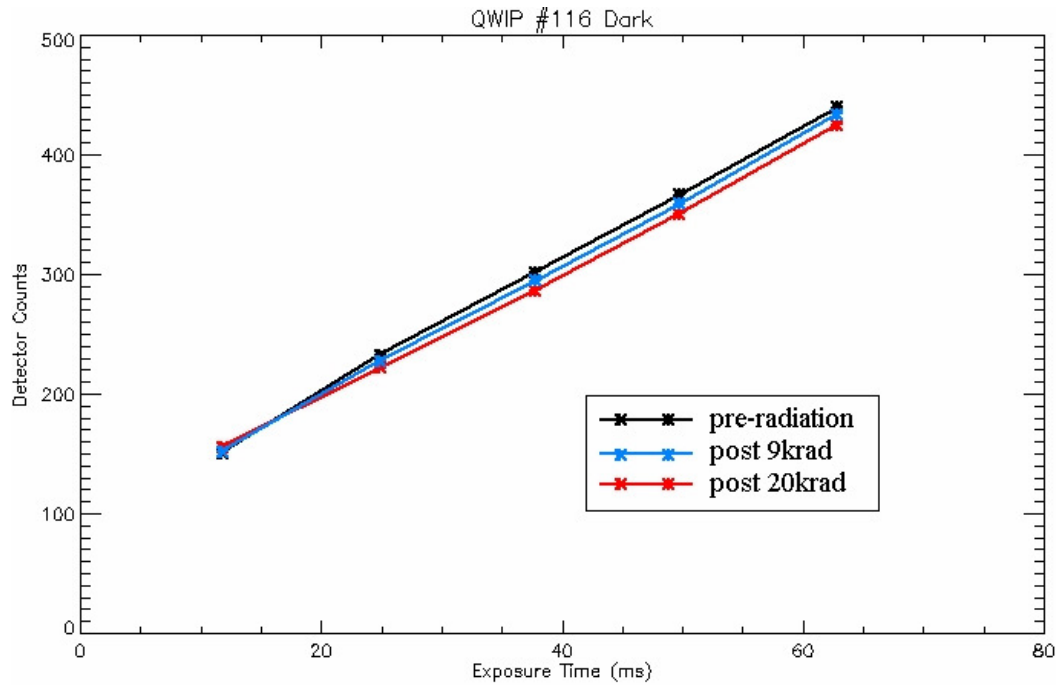


Fig. 2 Dark current signal versus exposure time as measured before, during and after proton irradiation for Q116. The median value of the full frame is plotted.

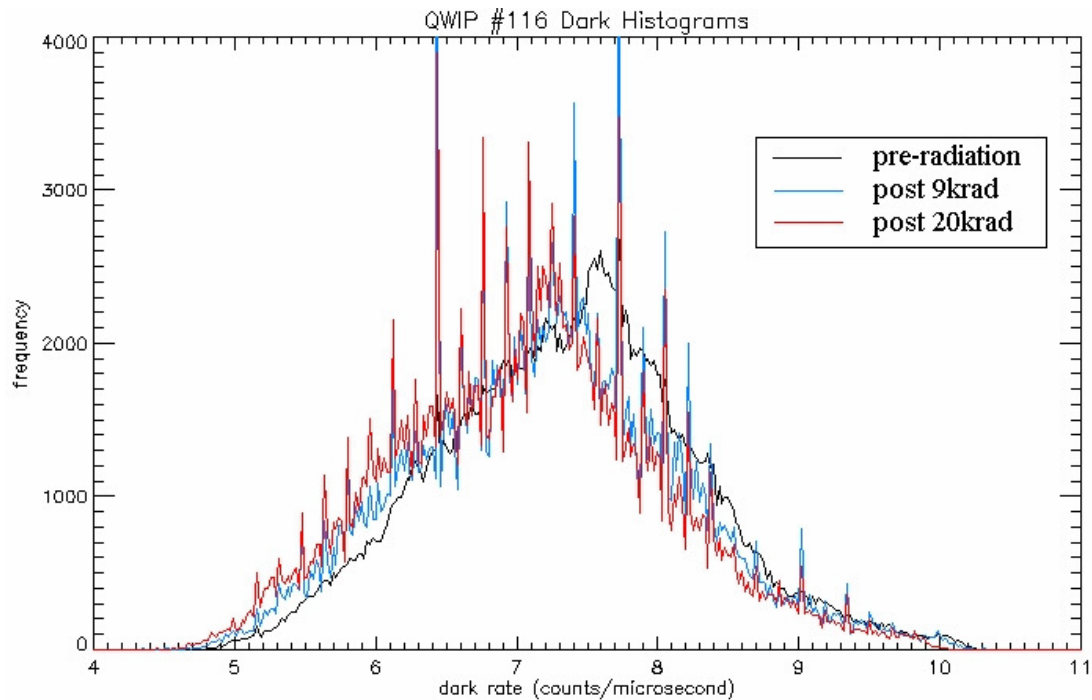


Fig. 3a Dark current histograms as measured before, during and after proton irradiation for Q116. The spikes in the histogram are due to spurious effects and nonlinearities in the SEIR data acquisition system.

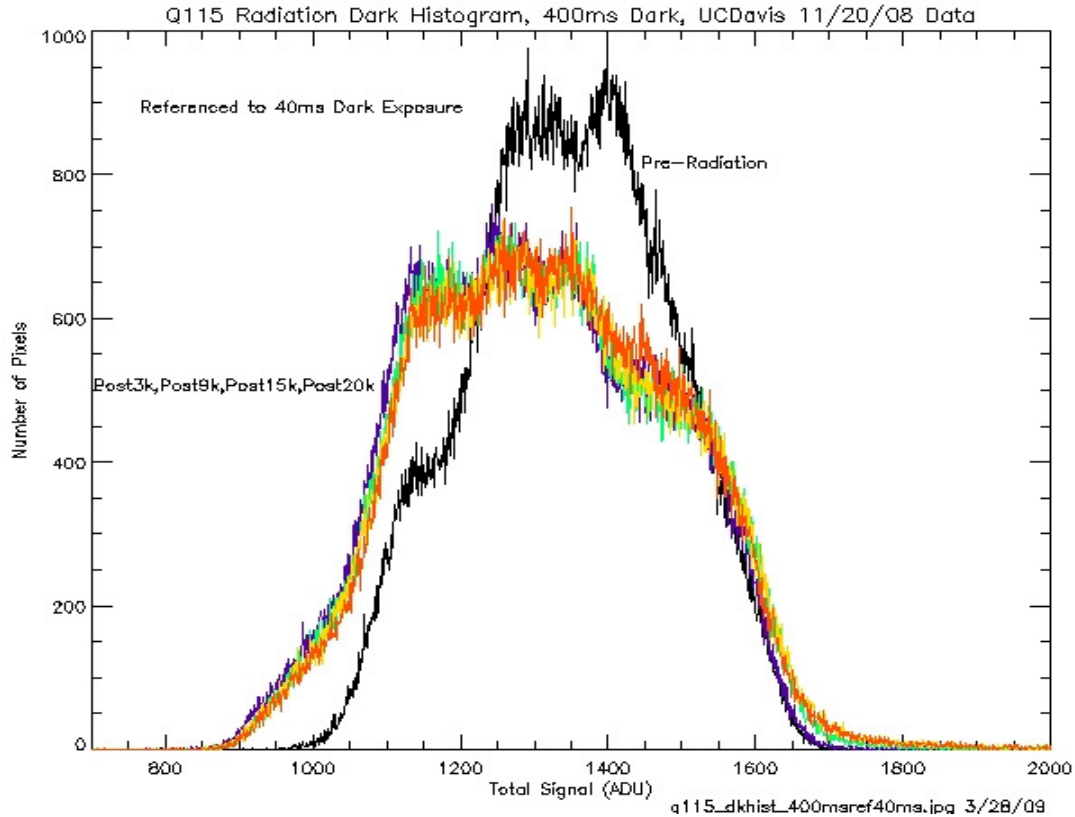


Fig. 3b Dark histograms as measured before, during and after proton irradiation for Q115.

Test results – Noise:

The noise was calculated from short dark exposures by subtracting two neighboring frames, building histogram of pixel values in the image differences, and then computing the histogram parameters by estimating the parameters of a Gaussian fit. The SEIR system displayed a significant differential non-linearity that most likely originated in the A/D converter. This resulted in distortion of the histograms, and made it difficult to compare the noise between different stages of the experiment as shown in Fig. 4.

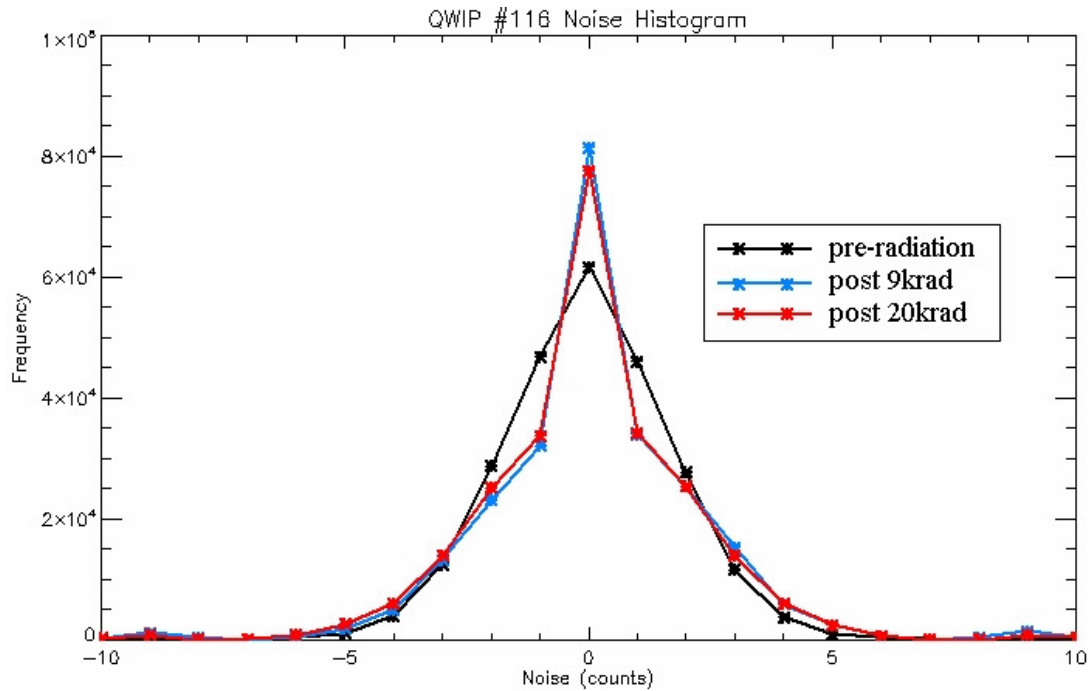


Fig. 4a Noise histograms as measured before, during and after proton irradiation for Q116. Distortions in the histograms are due to the differential nonlinearity in the SEIR data acquisition system.

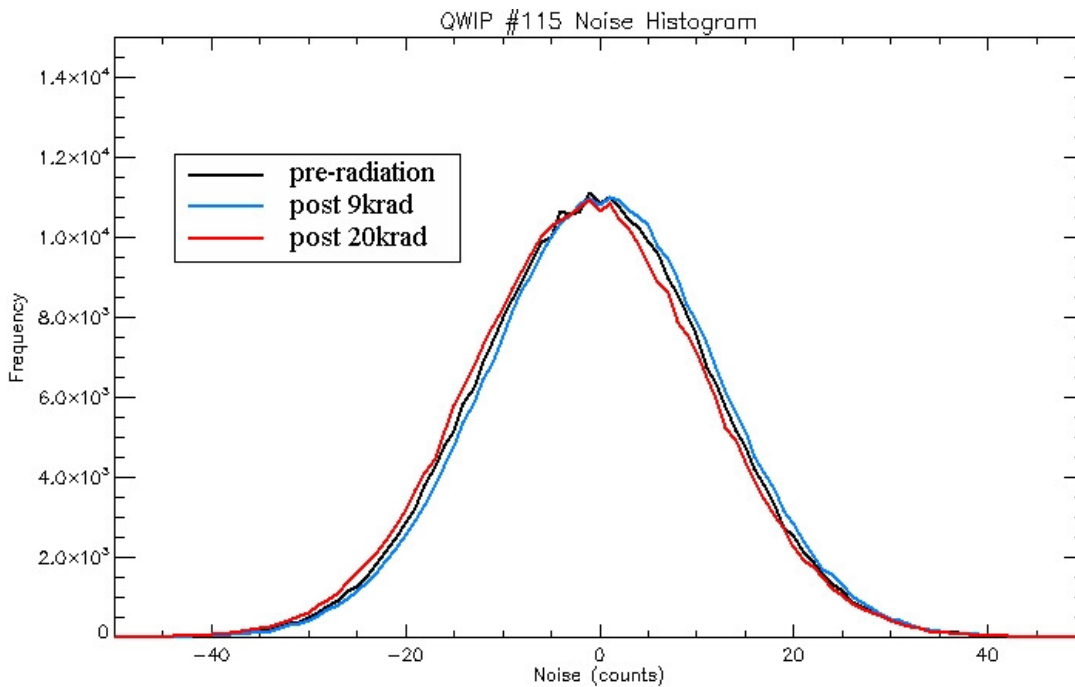


Fig. 4b Noise histograms as measured before, during and after proton irradiation for Q115 with the Leach controller.

Test results – Responsivity:

The ‘grey body’ source was placed behind the thermal shields to provide infrared radiation for the responsivity measurements. The black body was built from 100 Ω surface mount resistors, and its emissivity and color temperature were not calibrated. However, when powered with constant current, it exhibited reasonable stability and was used to monitor the detector response during irradiation. Fig. 5 shows the median value of the image resulting from grey body illumination as a function of exposure time measured before, during and after the proton irradiations. The results show good agreement despite the highly non-uniform illumination as depicted in Fig. 6. Fig. 7 shows histograms of the illuminated images before and after irradiation for both SCAs.

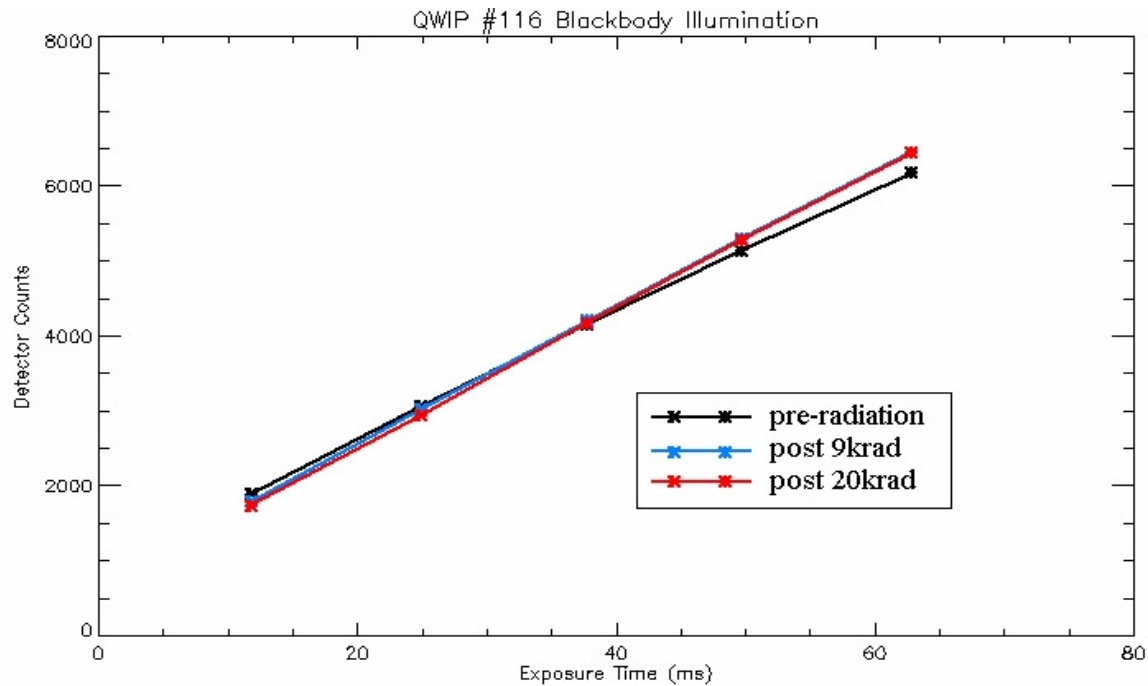


Fig. 5 The black body signal versus exposure time as measured before, during and after proton irradiations for Q116.

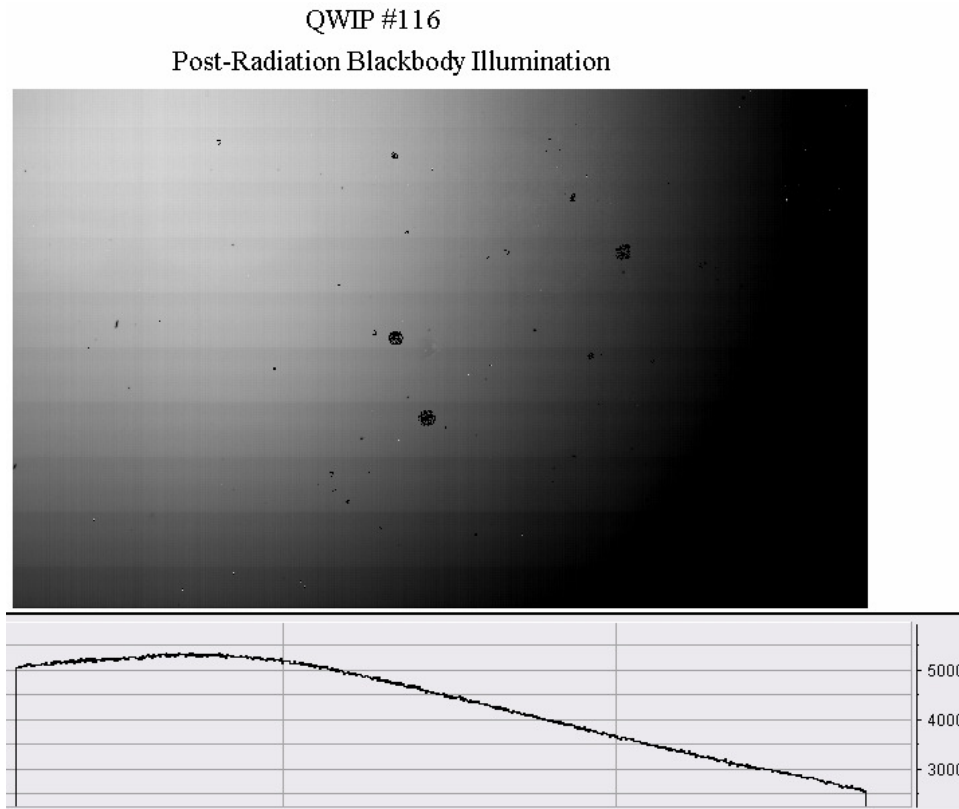


Fig. 6. The flat field image resulting from the black body source. The high non-uniformity resulted from the close and off axial placement of the black body emitter.

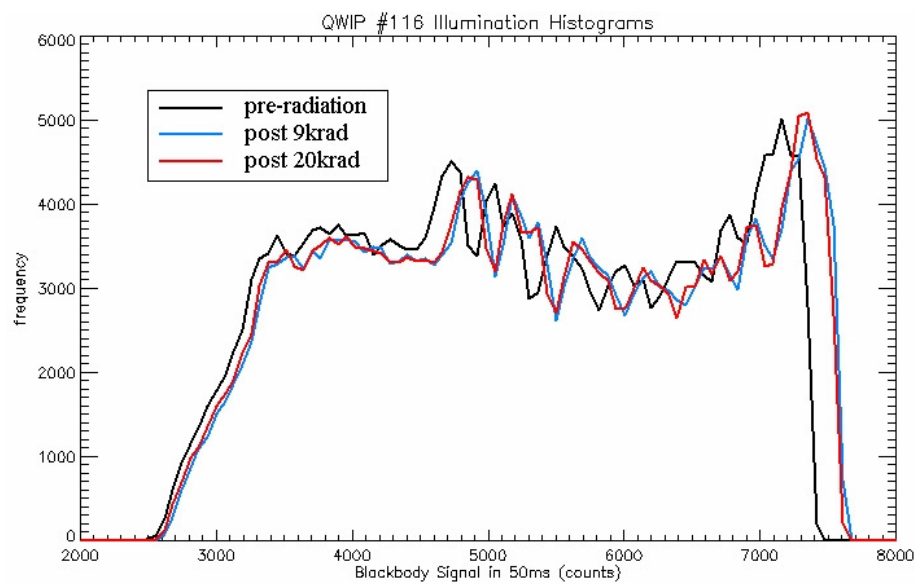


Fig. 7a Histograms of the illuminated images as measured before, during and after proton irradiations for Q116.

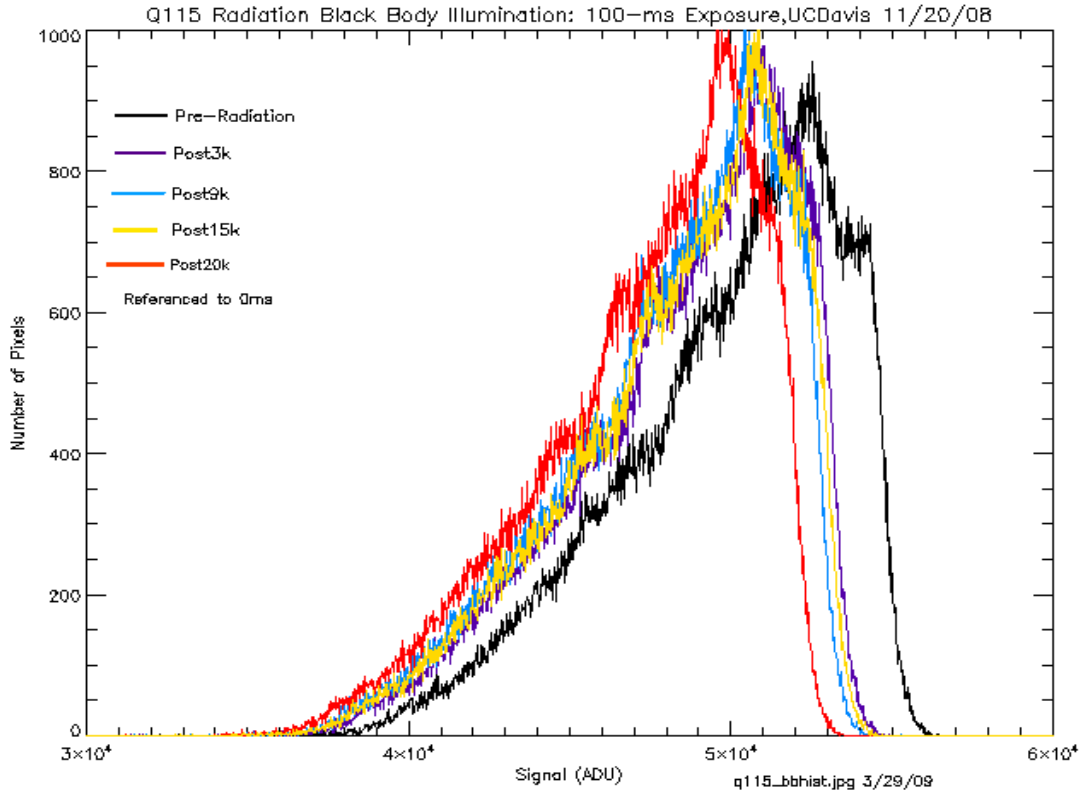


Fig. 7b Histograms of the illuminated images as measured before, during and after proton irradiations for Q115.

Test Results – Nonfunctional pixels:

It is well known that protons can cause permanent damage to the crystal structure which can result in the alteration of the detector pixel performance, especially highly increased dark currents (so-called hot pixels) and elevated noise in pixels. In addition, another research group has recently observed nonfunctional pixels in MUXES as a result of heavy ion radiation. It is possible that proton nuclear reaction fragments (which have much higher LETS than the incident protons) would be able to produce hot pixels. Further analysis is underway to understand the role of the QWIP detector versus the ROIC with respect to irradiation induced nonfunctional pixels. Nonfunctional pixels are defined here as pixels with a dark current higher than twice the mean dark or as pixels with a responsivity lower than 0.4 of mean responsivity.

Illuminated and dark images were used to compute number of nonfunctional pixels, and the results before and after proton irradiation were compared. As shown in Table 1, the number of nonfunctional pixels in the SCA, QWIP #116, remained unchanged throughout proton irradiation experiment. The statistics of the nonfunctional pixels in Table 1 was limited to the subset of the image from row 1 to row 390 since SEIR system was not imaging from row 391 to row 512. However, as illustrated in Table 2, Q115 exhibited a noticeable increase in the number of randomly distributed pixels with higher dark current. In both tables, the post anneal measurements were completed at GSFC after the devices had spent time at room temperature.

Table 1:

QWIP #116

Nonfunctional Pixels

| Time | Readout | Hot Pixels | Cold Pixels | TOTAL | % |
|-------------|---------|------------|-------------|-------|--------|
| Pre-Rad | SEIR | 4 | 423 | 427 | 0.173% |
| Post-9krad | SEIR | 8 | 425 | 433 | 0.175% |
| Post-20krad | SEIR | 8 | 422 | 430 | 0.174% |
| Post-20krad | Leach | 11 | 417 | 428 | 0.173% |
| Post-anneal | Leach | 5 | 414 | 419 | 0.170% |

Table 2:

QWIP #115

Nonfunctional Pixels

| Time | Readout | Hot Pixels | Cold Pixels | TOTAL | % |
|-------------|---------|------------|-------------|-------|--------|
| Pre-Rad | Leach | 6 | 4 | 10 | 0.003% |
| Post-3krad | Leach | 27 | 5 | 32 | 0.010% |
| Post-9krad | Leach | 85 | 5 | 90 | 0.027% |
| Post-15krad | Leach | 141 | 5 | 146 | 0.045% |
| Post-20krad | Leach | 161 | 5 | 166 | 0.051% |
| Post-anneal | Leach | 10 | 5 | 15 | 0.005% |

Test results – Transients:

A significant effort was undertaken to obtain the possible detailed signatures of the detector response to single proton events. On the first day, attempts to measure transients with the SEIR system during low proton flux exposures at 63.3 MeV were unsuccessful. The presence of proton events was demonstrated by increased noise observed, but single proton transients were too small to be distinguished from the noise in the pixels. On the second day, the proton beam energy experienced by the device was reduced to 9 MeV to increase the chances of transient detection (due to the increased LET of lower energy proton beams), and the Leach controller was used. Under these conditions, images of the Q115 array showed clear signatures of proton transients as demonstrated in Fig. 8. Using the Leach controller, the beam energy was returned to 63.3 MeV, and the low flux illuminations were repeated. This time, the transients were clearly detectable, and it was concluded that initial absence of the transients was solely due to the degraded response of SEIR system.

After the initial transient testing, the proton flux was increased to the levels necessary to keep radiation times reasonably short, yet low enough to avoid detector saturation for all integration times employed. Images were collected during each incremental irradiation, culminating in a total ionizing dose of 20 krad(Si), which corresponds to a fluence of 1.5×10^{11} 63.3 MeV protons per cm^2 .

For the low proton flux images, the density of protons was close to 1 per 50 pixels per 10 ms exposure. The protons produced transients with both positive and negative polarizations as shown by histograms in Figs. 8 - 11. We believe that the negative transients were the result of proton interactions with the multiplexer circuitry, whereas the positive transients represented a combination of the detector layer response and the multiplexer response. It appears that the negative transients involve fewer pixels per event as shown in Fig. 11. This is probably because they are likely to occur in a specific time and location with respect to the multiplexer circuitry. The positive events show more pixels involved in an average transient as some of them originate in the detector layer, and are therefore likely to cross pixel boundaries. The magnitude of the pulses did not exceed 1,500 counts in either direction.

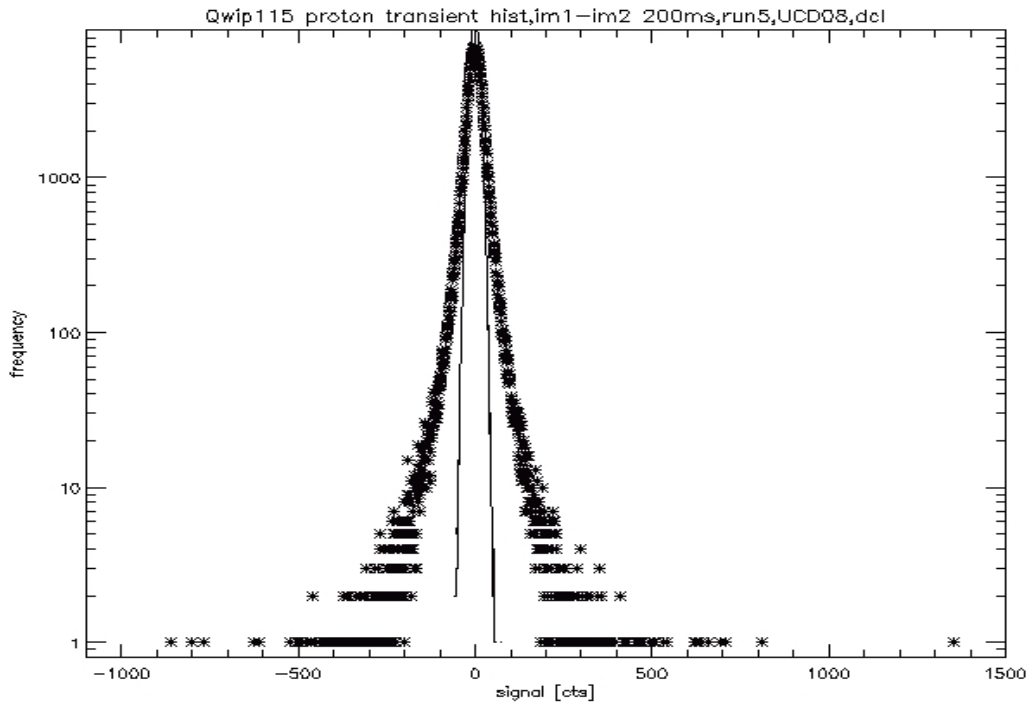


Fig. 8 Histogram of 63 MeV proton transients in low flux level images (stars) as compared to the noise histogram (solid line). The histograms are symmetrical since they represent the distribution of the difference of two images, both with proton transients.

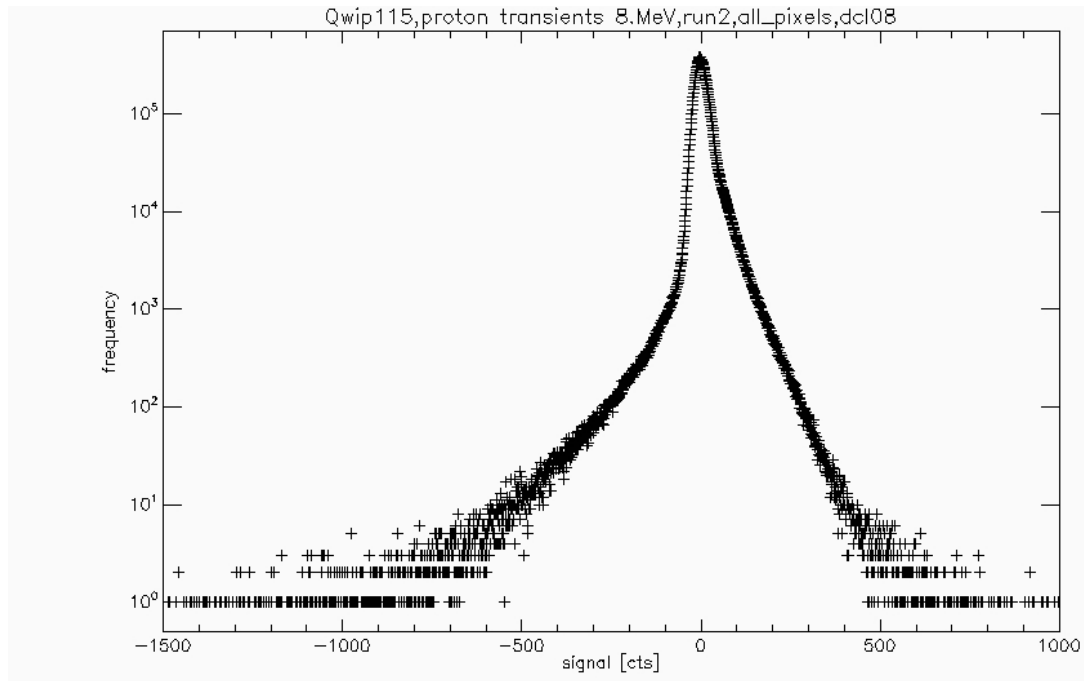


Fig. 9 Histogram of 9 MeV proton transients in low flux level images. Both negative and positive spikes are observed. The spike magnitudes do not exceed 1,500 counts.

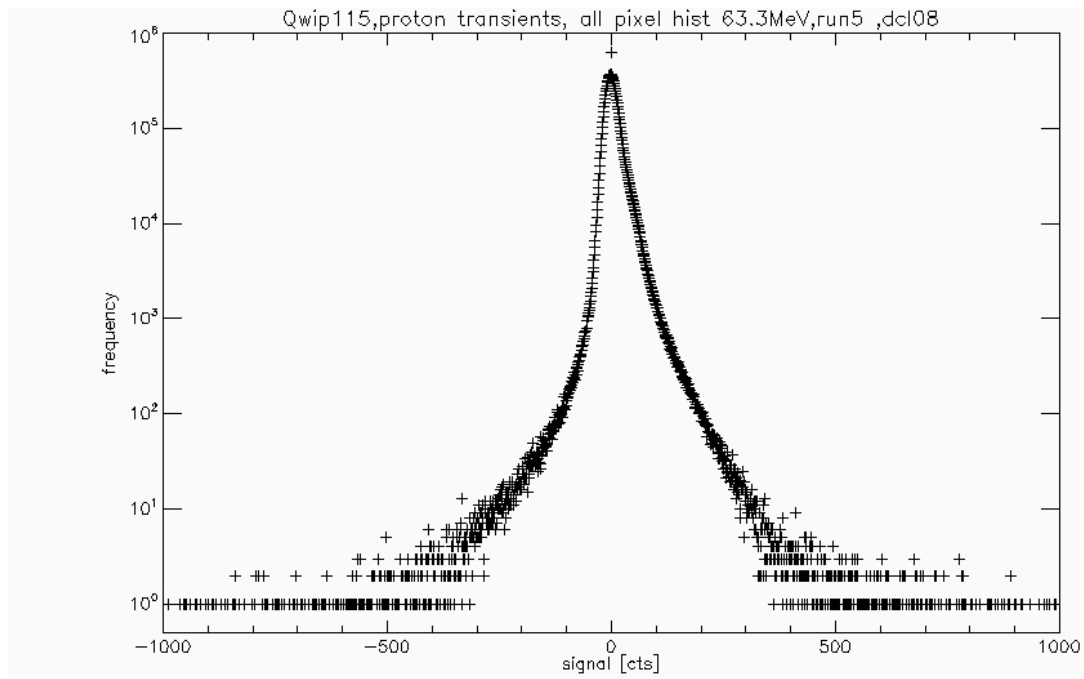


Fig. 10 Histogram of 63.3 MeV proton transients in low flux level images. Both negative and positive spikes are observed. The spike magnitudes do not exceed 1,500 counts.

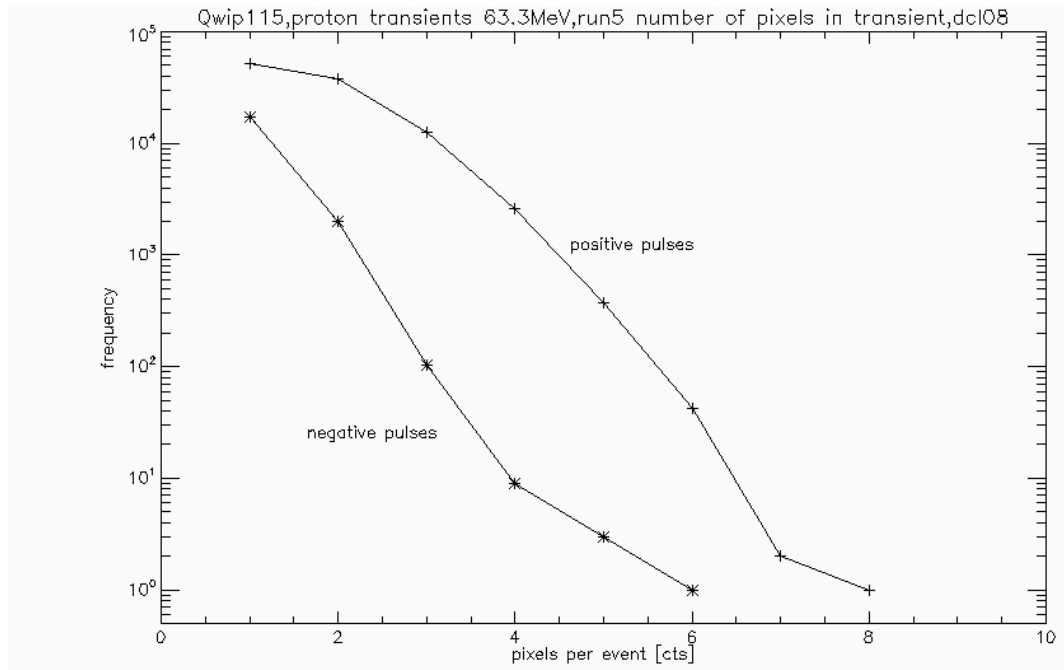


Fig. 11 Histogram of the number of pixels involved in proton transients in the low flux level images. The negative events affect fewer pixels than the positive events.

At higher proton flux levels corresponding to a density in the order of 10 protons per pixel per 10 ms exposure, higher magnitude transients were observed as shown in Fig. 12. Their magnitudes exceed 10,000 counts, and they display a dual polarity as was the case for the low flux transients. Table 3 gives an example of a large transient distribution as observed in run 7 for Q115. In this case, the radiation exposure of duration 225 seconds corresponded to a fluence of 4.7×10^{10} protons per cm^2 . With respect to the SCA, this translated into 1.8×10^6 protons per cm^2 per 10 ms exposure. As shown in Fig. 12, the noise in the high proton flux images was significant primarily due to the proton statistics. The standard deviation of this image was used to identify large events as those which deviated from the mean by more than n -sigma in either the positive or negative direction.

Table 3 Statistics of the large magnitude transients.

| Detection level Standard deviation | Detected number of events | Probability of large transient (per proton) |
|---------------------------------------|------------------------------|--|
| 3 | 3505 | 1.2e-5 |
| 4 | 1165 | 4.0e-6 |
| 5 | 642 | 2.2e-6 |
| 6 | 459 | 1.6e-6 |
| 7 | 360 | 1.2e-6 |
| 8 | 291 | 1.0e-6 |

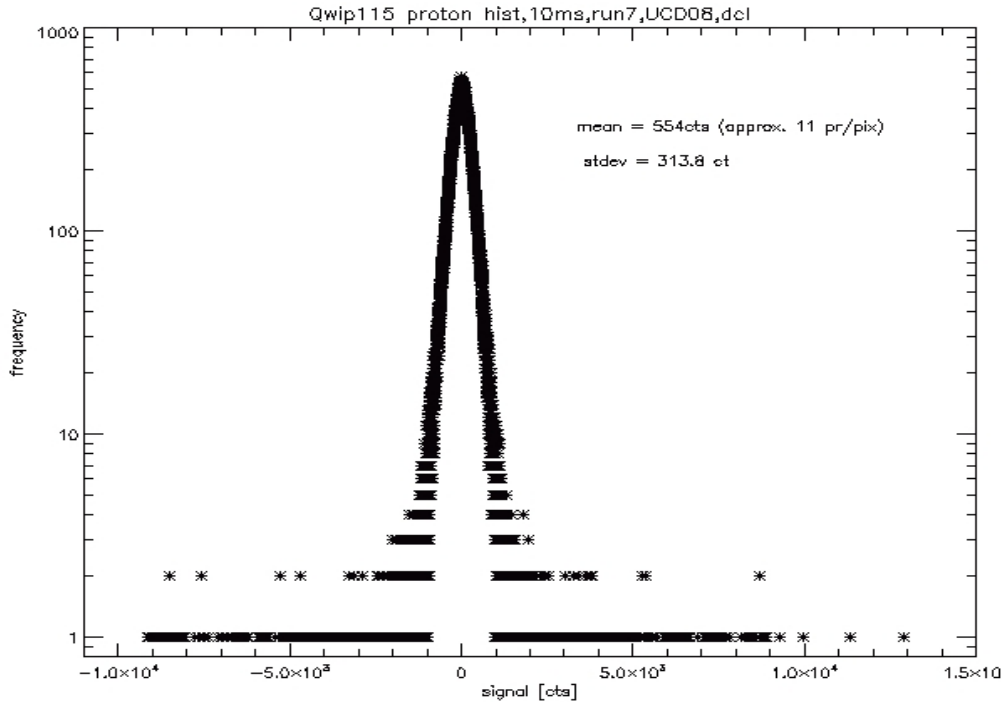


Fig. 12 Histogram of 63.3 MeV proton transients in high proton flux images corresponding to approximately 11 protons per pixel per exposure. Both negative and positive spikes are observed. The spike magnitudes reach 10,000 counts.

Fig. 13 is an image collected during a high proton flux exposure. The white points represent high magnitude transients. As can be seen in the image, they initiate a darker stripe along the column direction following the event. Notice that the readout direction is from the bottom to top of the image in Fig. 13. Typically, a large positive going transient triggers a column shift in the negative direction as shown in Fig. 14. This shift tends to persist for the remaining rows in the image, and eventually is 'reset' to the nominal level for the next image frame. It should be noted that the multiplexer configuration is reset to the 'user set' multiplexer configuration before each frame acquisition. Fig. 15 represents a column average of the proton image compared with the same average once proton beam has been stopped (as shown in the lower trace). It is worth noting that the negative going spikes in the column profile are opposite to the positive spike which triggers the event.

As the frame readout progresses, more and more of the large events occur and more columns get shifted down. This effect can be seen in the profile of the row average illustrated in Fig. 16. Large transients produced by the protons appear to interact primarily with the multiplexer readout and indicate sensitivity of this design to the space radiation environment.

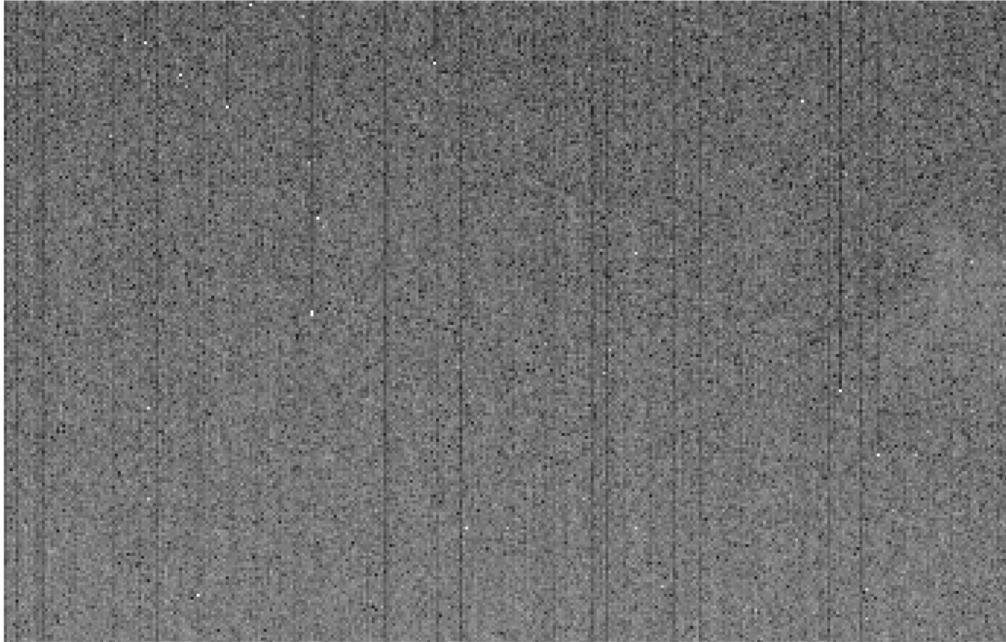


Fig. 13 Image of transient events produced during a high proton flux. The high amplitude spikes trigger a column shift seen as the dark vertical lines.

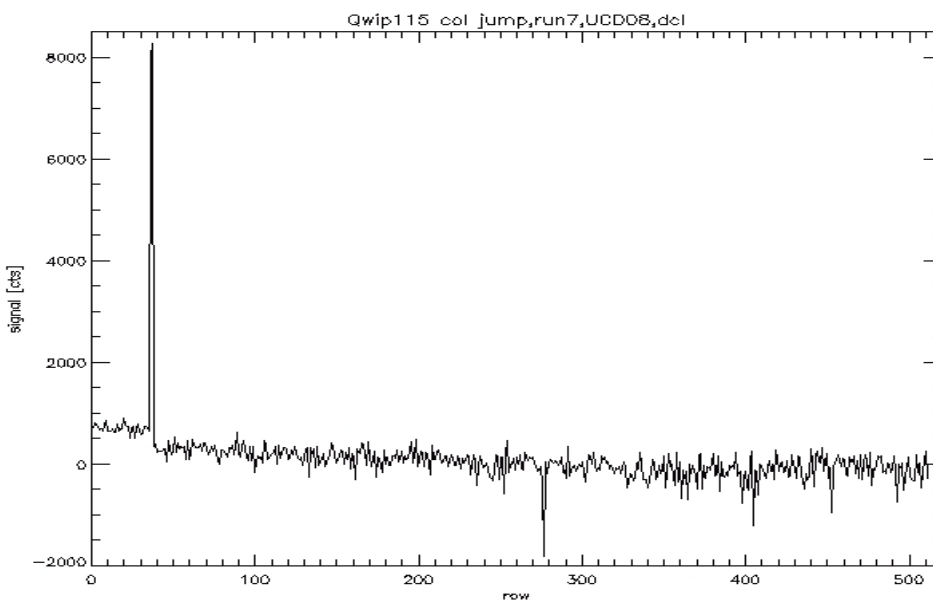


Fig. 14 A column shift triggered by a large proton transient. The column shift is opposite to the transient direction, and persists until the end of the frame.

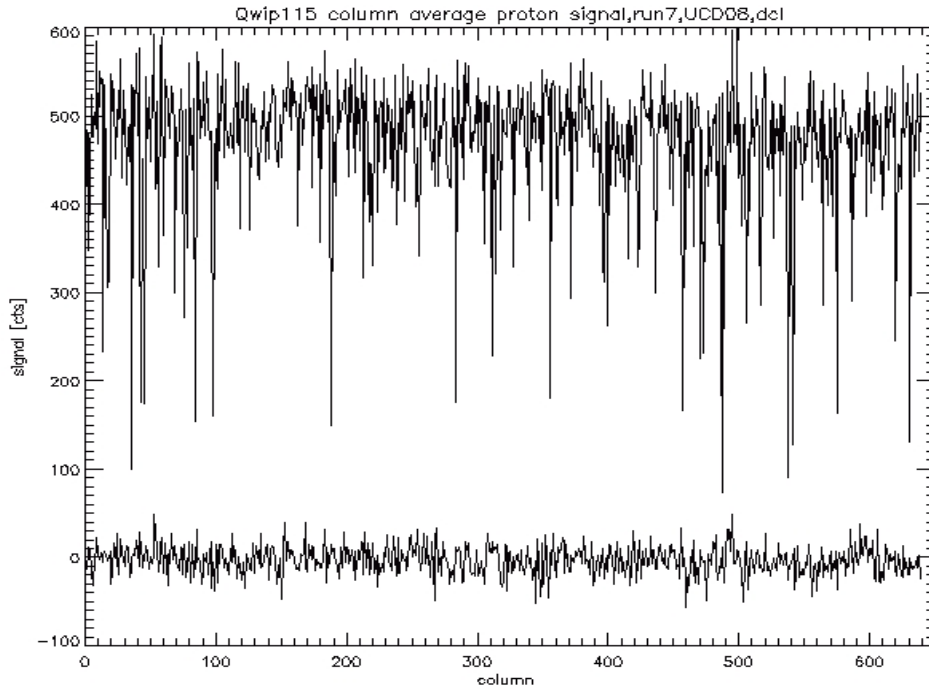


Fig. 15 Comparison of the column average in the proton image (upper trace) with the proton free image (lower trace). The large negative spikes correspond to the dark traces induced mostly by positive proton transients.

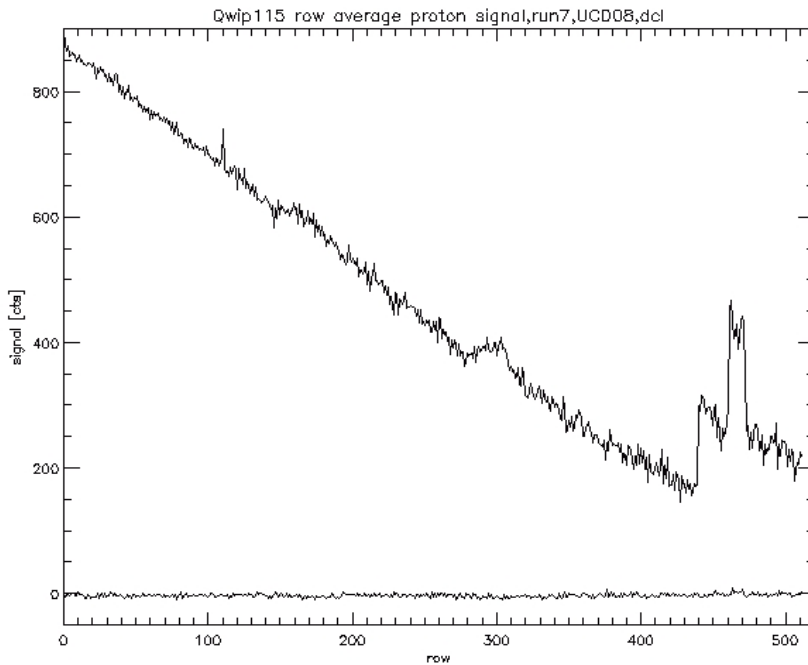


Fig. 16 The mean row profile observed in the high proton flux image. The dramatically reduced signal at the end of the image is due to the increased number of columns shifted down due to the transient. The lower trace shows the same row profile for the image after the proton beam is turned off.

Fig. 17 illustrates the evolution of the mean signal during a proton exposure of approximately 3 minutes duration. At the beginning, the mean row signal stays constant at the pre-irradiation level. (The figure shows the difference between the observed row mean and that measured before the radiation exposure.) As soon as the beam is turned on, the signal increases and, in follow up images keeps ramping down as shown in Fig. 16. After each frame, a new configuration command is sent to the multiplexer and the signal partially returns to the original level, but not entirely. At the end of the proton exposure (~3 minutes), the row mean is 500 counts (or 50,000 electrons) above the level when the proton beam is first turned on. The signal level shift due to the irradiation remains even after the proton beam is switched off (see the blue portion of Fig. 17), and is removed only after a power cycle is implemented (see the brown section in Fig. 17). It appears that readout switches into a different mode of operation which cannot be restored to normal operation by the serial word command. Instead, it is necessary to cycle power in order to return to normal operation.

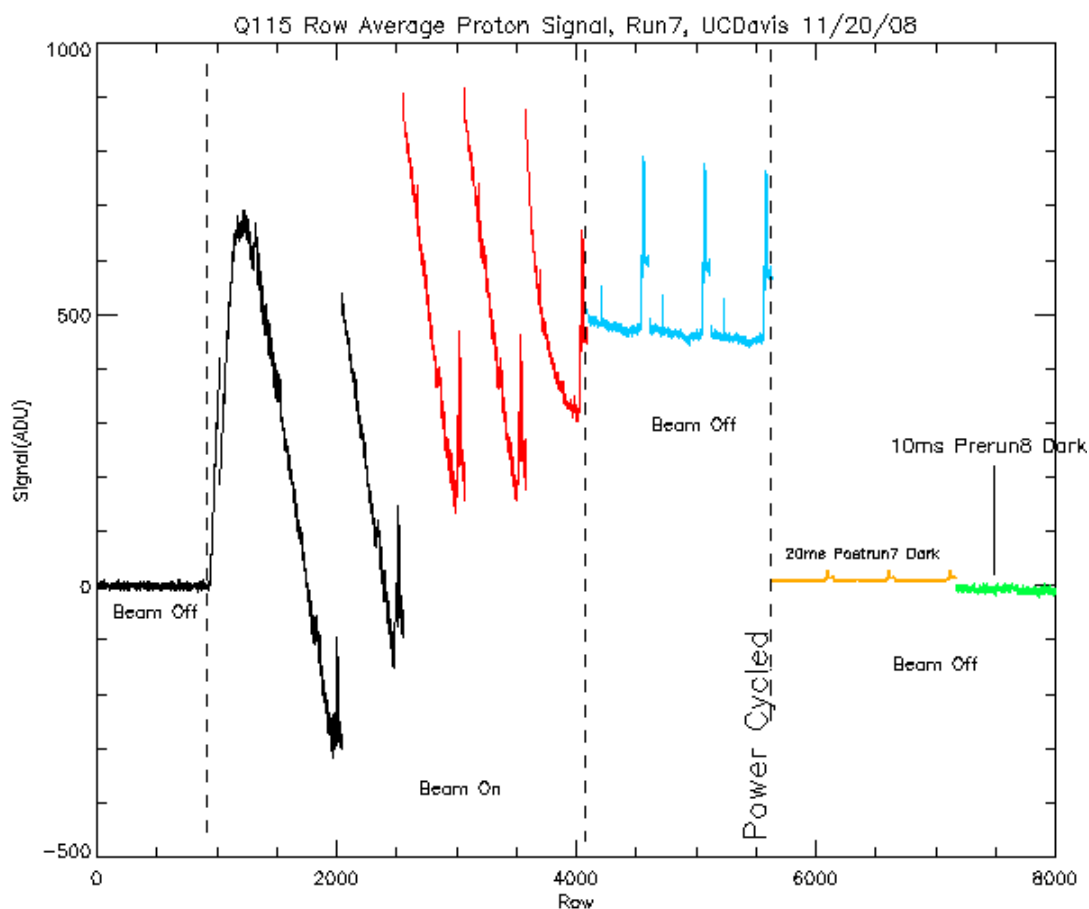


Fig. 17 The mean row profile observed in the high proton flux images. Selected images from a sequence of 250 frames are shown. The first section (0 to 1024) shows two frames before the beam is turned on, followed by a few frames with beam on (shown in black). A few frames before the beam is turned off are shown in red, followed by 3 frames in blue after the proton beam has been turned off. Next, the implementation of a power cycle is indicated, after which there are 3 dark frames with 20ms exposures (in brown), and finally 2 dark frames with 10 ms exposure shown in green.

Conclusions:

1. Two QWIP detectors (Q115 and Q116) were exposed to 20 krad(Si) equivalent of 63.3 MeV proton radiation, corresponding to a fluence of 1.5×10^{11} protons/cm². The SCAs exhibited no change of dark current, noise or responsivity as compared to that observed before proton irradiation. Q115 exhibited a consistent increase in the number of hot pixels as a function of increasing proton fluence, but no such effect was observed for Q116. The low number of hot pixels observed, even at the 20 krad(Si) level, is not expected to present a problem for TIRS, but it is noted that the hot pixels are successfully annealed after a room temperature anneal. It is also relevant that the proton test was performed using standard 1019.7 procedures to the maximum extent possible, and hence provided further evidence of the very robust TID response of the MUX, although these parts were not flight lot parts.
2. The images collected during proton irradiation have shown a sensitivity of the ICS9803 readout to proton bombardment. Large transients occur with probability of $\sim 1 \times 10^{-6}$ per incident proton, which corresponds to the rough probability expected for a proton nuclear reaction event within the device. Such reactions result in higher LET nuclear reaction products which would be expected to be more likely to produce an SEE event in the multiplexer. (See Appendix II for more discussion.) The large transients tend to produce negative column shifts that result in a significant alteration to the collected images. Nevertheless, so far, it has been observed that the column offsets correct themselves prior to a new frame. Note that before each new frame, commands are sent to the MUX to set the configuration to the command mode, set the gain at 1.33, and the mode to “integrate then read.” This is believed to represent a relevant mode of operation of the MUX. Based on information from FLIR, this procedure automatically resets the logic portion of the MUX circuitry. Nevertheless, a full disclosure of the extent of the effective reset of the MUX circuitry in this mode of operation has not been received from FLIR. Although some of the analog circuitry (e.g. current sources and amplifiers) can never be reset, the optimal operational mode with respect to SEE effects is still in discussion with FLIR.

The mechanism for the observed proton induced row baseline offset is not currently understood. We have discussed this SEE observation with Jim Woolaway at FLIR, and he cannot discern how the design of the Indigo 9803 can result in this effect, especially given the configuration of the timing circuitry for the chip. Further examination of the current proton data set to confirm whether the baseline offset *only* corrects at the end of frame, and also details of the shape of the offset correction in the case that it is observed to correct *before* the end of a frame, may provide some useful clues.

To fully understand the nature of the SEE response that requires a power cycle, as illustrated in Fig. 17, further investigation is required.

Appendix I Beam Dosimetry

The dosimetry system has been well characterized at UC Davis CNL. Periodically, and after each beam current or proton energy change, the Faraday Cup (FC) to Secondary Electron Monitor (SEM) ratio was measured to verify that the proper proton beam and internal vacuum were in place.

Table 1 Q116 dosimetry and run notes. All exposures are for 63.3 MeV protons.

| Date | Run Notes | Run # | Beam Current (pA) | Beam Flux (p/cm ² /s) | Exposure Time (sec) | Increment. TID (Rad(Si)) | Cumulat. TID (rad(Si)) | Increment. Fluence (p/cm ²) | Cumulat. Fluence (p/cm ²) |
|---------|--|-------|-------------------|----------------------------------|---------------------|--------------------------|------------------------|---|---------------------------------------|
| | Determine the best integration time; 120 ms | | | | | | | | |
| 9/19/08 | integration; manual stop | 1 | 0.81 | 1.38E+05 | 26.7 | 4.94E-01 | 4.94E-01 | 3.69E+06 | 3.69E+06 |
| 9/19/08 | 1 ms; SEIR until noted. | 2 | 0.69 | 1.17E+05 | 9.2 | 1.45E-01 | 6.38E-01 | 1.08E+06 | 4.77E+06 |
| 9/19/08 | 10 ms | 3 | 0.6 | 1.03E+05 | 21.4 | 2.95E-01 | 9.33E-01 | 2.21E+06 | 6.97E+06 |
| 9/19/08 | 120 ms | 4 | 3.52 | 6.01E+05 | 31.9 | 2.57E+00 | 3.50E+00 | 1.92E+07 | 2.61E+07 |
| 9/19/08 | 120 ms | 5 | 3.24 | 5.53E+05 | 7.42 | 5.49E-01 | 4.05E+00 | 4.10E+06 | 3.02E+07 |
| 9/19/08 | 120 ms | 6 | 25.2 | 4.08E+06 | 31.9 | 1.74E+01 | 2.15E+01 | 1.30E+08 | 1.60E+08 |
| 9/19/08 | 120 ms, repeat | 7 | 18.1 | 3.09E+06 | 10.95 | 4.53E+00 | 2.60E+01 | 3.38E+07 | 1.94E+08 |
| 9/19/08 | 120 ms, repeat | 8 | 23.8 | 4.06E+06 | 33.7 | 1.83E+01 | 4.43E+01 | 1.37E+08 | 3.31E+08 |
| 9/19/08 | 120 ms; preset dose | 9 | 196 | 3.35E+07 | 218 | 9.77E+02 | 1.02E+03 | 7.30E+09 | 7.63E+09 |
| 9/19/08 | 120 ms | 10 | 196 | 3.34E+07 | 220 | 9.83E+02 | 2.00E+03 | 7.34E+09 | 1.50E+10 |
| 9/19/08 | 10 ms | 11 | 1030 | 1.76E+08 | 297 | 7.00E+03 | 9.00E+03 | 5.23E+10 | 6.73E+10 |
| 9/19/08 | 10 ms | 12 | 1030 | 1.76E+08 | 255 | 6.00E+03 | 1.50E+04 | 4.49E+10 | 1.12E+11 |
| 9/19/08 | 10 ms | 13 | 1050 | 1.79E+08 | 208 | 5.00E+03 | 2.00E+04 | 3.73E+10 | 1.49E+11 |
| | Check transients with Leach controller; 10 ms & 100 ms integrations; Goal to differentiate proton hits | | | | | | | | |
| 9/20/08 | to MUX vs. QWIP | 14 | 0.968 | 1.65E+05 | 60.4 | 1.33E+00 | 2.00E+04 | 9.96E+06 | 1.49E+11 |
| | 200 ms & "0" ms | | | | | | | | |
| 9/20/08 | integration | 15 | 3.19 | 5.44E+05 | 1171 | 8.53E+01 | 2.01E+04 | 6.37E+08 | 1.50E+11 |

Table 2 Q115 dosimetry and run notes. All exposures are for 63.3 MeV protons, except as noted otherwise. TID and fluence dosimetry are reset starting with run 4 because the earlier runs have *very* low fluxes, and because as a result of intracolumnar recombination at 9 MeV, the TID delivered was negligible. All data were acquired using the Leach controller.

| Date | Run Notes | Run # | Beam Current (pA) | Beam Flux (p/cm ² /s) | Exposure Time (sec) | Increment. TID (Rad(Si)) | Cumulat. TID (rad(Si)) | Increment. Fluence (p/cm ²) | Cumulat. Fluence (p/cm ²) |
|---------|---|-------|-------------------|----------------------------------|---------------------|--------------------------|------------------------|---|---------------------------------------|
| 9/20/08 | 9 MeV protons; 10 ms & 120 ms integration; manual stop | 1 | 1.05 | 1.78E+05 | 59.1 | 6.15E+00 | 6.16E+00 | 1.05E+07 | 1.06E+07 |
| 9/20/08 | 9 MeV protons; 10 ms & 120 ms integration; Increase statistics | 2 | 1.07 | 1.82E+05 | 363 | 3.85E+01 | 4.47E+01 | 6.60E+07 | 7.66E+07 |
| 9/20/08 | 10 ms & 120 ms integration | 3 | 0.973 | 1.66E+05 | 80.9 | 1.80E+00 | 1.80E+00 | 1.34E+07 | 1.34E+07 |
| 9/20/08 | Varied exposure times during irradiation to help distinguish between MUX vs QWIP hits. (Shortest exposure favors seeing MUX hits.) Dosimetry reset. | 4 | 1.02 | 1.73E+05 | 617 | 1.43E+01 | 1.61E+01 | 1.07E+08 | 1.20E+08 |
| 9/20/08 | Increase statistics | 5 | 2.04 | 3.48E+05 | 380 | 1.77E+01 | 3.38E+01 | 1.32E+08 | 2.53E+08 |
| 9/20/08 | 200 ms integration time; preset dose | 6 | 606 | 1.03E+08 | 214 | 2.96E+03 | 3.00E+03 | 2.21E+10 | 2.24E+10 |
| 9/20/08 | 200 ms | 7 | 1030 | 1.75E+08 | 255 | 5.99E+03 | 8.99E+03 | 4.48E+10 | 6.72E+10 |
| 9/20/08 | 200 ms | 8 | 1020 | 1.73E+08 | 259 | 6.00E+03 | 1.50E+04 | 4.48E+10 | 1.12E+11 |
| 9/20/08 | 200 ms | 9 | 1020 | 1.74E+08 | 215 | 5.00E+03 | 2.00E+04 | 3.73E+10 | 1.49E+11 |

Appendix II:

Implications of the Present Proton Test for the Heavy Ion Response of the SCA

As a part of the proton test, we exposed the SCAs to approximately twice the mission TID level in order to monitor the Indigo 9803 MUXES for possible single event effect (SEE) effects. During proton irradiation at 63 MeV, a very small, but significant number of nuclear reactions occur that produce heavy ion fragments that are highly ionizing. If such a fragment strikes a sensitive portion of a MUX, there is the potential to produce an SEE that causes some type of mode change in the MUX, for example, a miss-registration of rows or columns, or a current change, etc. Although such observations can give us a flavor of the possible heavy ion induced SEE responses of the devices, they cannot be readily used to make predictions of the device response to the cosmic ray environment¹, because the spectrum of LETs generated by nuclear reaction events is much different than the on-orbit heavy ion LET spectrum. One important difference is that the proton reaction induced LETs are generally much lower than those experienced on-orbit. Also, proton exposures give *no* indication of the single event latch-up susceptibility of the parts. Nevertheless, this was a useful test for two main reasons (1) the TIRS orbit is a polar orbit with a significant cosmic ray exposure, and (2) there is very sparse data on heavy ion (or proton) induced SEE effects in MUXES.

As discussed in the transient test results section of this report, we observed “row offsets” that occurred with the same frequency expected for the proton induced nuclear reaction events. These events appear to resolve as a consequence of the routine sequence to set up the SCA for a new frame. However, in some cases a power cycling is required to restore normal operation of the SCA. The frequency of the later events is not currently known.

In general, we do not expect the frequency of on-orbit of cosmic ray induced SEE events to be large, but recommend that the project understand the nature and variety of the SEE events that may occur. It is useful to understand whether they self correct between frames, require a power cycle, or may produce permanent damage.

¹ There is literature that attempts to predict the heavy ion SEE (excluding latch-up, and other destructive SEEs) response based on 200 MeV proton data. However, the majority of this work was specifically calibrated for the International Space Station (ISS) orbit. This approach resolved some practical test issues for the ISS program, but remains controversial in general. The specific results for ISS related investigations do not apply to other orbits.